Topology optimization of inertia driven dosing units

Andreasen, Casper Schousboe

Published in:
Structural and Multidisciplinary Optimization

Link to article, DOI:
10.1007/s00158-016-1573-4

Publication date:
2017

Document Version
Peer reviewed version

Structural Multidisciplinary Optimization manuscript No.
(will be inserted by the editor)

Topology optimization of inertia driven dosing units

Casper Schousboe Andreasen

Received: date / Accepted: date

Abstract This paper presents a methodology for optimizing inertia driven dosing units, sometimes referred to as eductors, for use in small scale flow applications. The unit is assumed to operate at low to moderate Reynolds numbers and under steady state conditions. By applying topology optimization to the Brinkman penalized Navier-Stokes equation the design of the dosing units can be optimized with respect to dosing capability without initial design assumptions. The influence of flow resistance and speed is investigated to assess design performance under varying operating conditions.

Keywords Topology Optimization · Navier-Stokes · flow optimization · nozzle · dosing unit · eductor

1 Introduction

In many flow applications dosing of a secondary fluid with almost identical properties to the primary fluid is needed. This could for instance be the dosing of a tracer dye or a solution of small tracing particles. From a processing point of view dispensing the secondary fluid should be associated with a minimum cost. One way of dispensing the secondary fluid is to use a pump to supply fluid into the primary flow. However, it is often much more economic to use a single pump and drive the dosing of a secondary fluid by the energy which is already in the primary flow. This is typically done as sketched in Fig. 1. A nozzle is used to accelerate the fluid flow and thus lowers the static pressure locally which in turn allows suction of the secondary fluid into the primary flow. The principle has been widely used in e.g. spray paint pistols and similar equipment and is, in the context where a fluid is used to drive another fluid, referred to as an eductor or a jet pump.

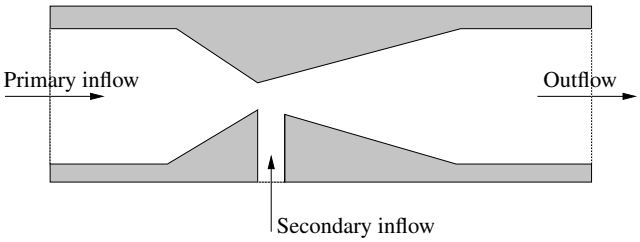

Fig. 1 Sketch of an inertia driven dosing unit. Left boundary is primary inflow. Right boundary is outlet. The secondary fluid enters from the lower port driven by the low static pressure right after nozzle.

The scope of this paper is to synthesize the design of these flow geometries by applying topology optimization to the Navier-Stokes equations in order to obtain optimized flow designs. This provides insight into the limiting factors and operating limits for the inertia driven dosing process. The performance limits and corresponding designs are investigated in order to assess the robustness of these optimized designs at varying flow conditions.

The design and optimization of flow devices based on nozzles have been of great interest both in an academic and an industrial context as they are applied in e.g. steam engines, jet engines for fuel supply (Hu et al, 1999) and in refrigeration plants. Optimization of axisymmetric nozzles for ejectors in the turbulent regime has furthermore been studied in e.g. Dvorák (2006); Fan et al (2011). Opposed to shape optimization where the shape of the boundary is parameterized this paper utilizes a method where the shape of the component is not predefined and the resulting design can have a different topology than the initial one.

Topology optimization originates from the solid mechanics community where it was first presented in the context of

C.S. Andreasen
Technical University of Denmark, Section for Solid Mechanics, Niels Koppels Allé, Building 404, DK-2800 Kgs. Lyngby, Denmark
E-mail: csan@mek.dtu.dk

homogenization methods for structural optimization problems (Bendsøe and Kikuchi, 1988). By representing the design in terms of single elements, like pixels in a digital image, the physics is modeled in the entire computational domain. By interpolating the material parameters e.g. density or porosity, either regions of material or void can be modeled and there is no need for an explicit boundary representation. This makes it easy to introduce new internal boundaries or make them disappear. The method has successfully been introduced into the optimization of materials and components in various physics such as optics, acoustics and flows due to its versatility (Bendsøe and Sigmund, 2003).

Optimization of designs related to fluid flow problems has been studied for decades before topology optimization was developed and optimal shapes for minimum dissipated power in Stokes flow have been determined analytically already in the 1970s by Pironneau (1973). The topology optimization of flow problems were first presented in the seminal paper by Borrvall and Petersson (2003) considering Stokes flow and further extended to Navier-Stokes flow, though still in the laminar regime in Gersborg-Hansen et al (2005). The optimization method has recently been extended to transient and dynamic flow problems (Kreissl et al, 2011; Deng et al, 2011) though still limited to laminar flows. Traditionally the finite element method has been used for the modeling of topology optimization problems; however, fluid flow problems have also been optimized using the finite volume method (Othmer, 2008), the Lattice-Boltzmann method (Pingen et al, 2007) and kinetic gas theory (Evgrafov et al, 2008). A few works on flow components that are able to pump a fluid and have been designed by topology optimization have been promoted. Impeller designs for flow machines have been studied by Romero and Silva (2014) and Andreasen et al (2014) for 2D and 3D designs, respectively. An alternative unsteady pump design is promoted by Nørgaard et al (2016). On top of the flow problems different transport phenomena have been considered i.e. passive transport (Andreasen et al, 2009), reacting flows (Okkels and Bruus, 2007), buoyancy problems (Alexandersen et al, 2014), active transport e.g. heat (Yoon, 2010a; Marck et al, 2013; Alexandersen et al, 2016). Models for including the fluid structure interaction have been developed as demonstrated in Yoon (2010b) and Kreissl et al (2010). In this work, the deformations of the component are assumed negligible, and thus the solid is assumed infinitely stiff and no interaction is modeled. Furthermore, the flow problem is assumed to be of small scale such that the flow is considered laminar and sufficiently slow and stationary such that it can be modeled under the assumption of steady-state. The designs considered are modeled as plane 2D flow problems; however, the presented methodology should be readily applicable for 2D axisymmetric and 3D flow models.

The paper is organized such that the method and the physics are described in section 2. The obtained results and numerical studies are presented and discussed in section 3 while the paper and its findings are concluded in section 4.

2 Method

The flow is modeled using the incompressible Navier-Stokes equations as the flow is assumed to be of low speed with a constant viscosity and of laminar nature. On the other hand, the inertia is important for the application as the secondary flow needs to be sucked in by a local low pressure generated by the inertia. Operation in the creeping flow limit is therefore not possible.

The topology optimization of the flow component is introduced into the model by adding a Brinkman term (Brinkman, 1947) to the Navier-Stokes equation. This allow control of the flow by mimicking a porous material. The Brinkman medium is slowing down the fluid by many orders of magnitude and in the limit representing a solid material. However, in the model the fluid is able to penetrate the medium at the cost of a huge pressure loss, so care should be taken to check the influence of possible flow in these regions of the final designs, c.f. Kreissl and Maute (2012) for further discussions. The steady state equations yield

$$-\nabla\cdot(\mu(\nabla\mathbf{u}+(\nabla\mathbf{u})^T)-\mathbf{I}p)+\mathbf{u}\cdot\rho\nabla\mathbf{u}+\alpha(\xi)\mathbf{u}=0 \qquad (1)$$

$$\nabla\cdot\mathbf{u}=0 \qquad (2)$$

where $\mathbf{u}$ is the velocity, p the pressure, μ the dynamic viscosity, ρ the mass density and α the Brinkman penalization parameter (inverse permeability) which is dependent on the spatial design field $\xi\in[0;1]$ where 0 represents solid material (black) and 1 represents fluid (white).

The domain considered for the modeling is shown in figure 2 where the boundary subsets are denoted. The boundary conditions yield

$$\mathbf{u}=\mathbf{0} \qquad \text{at } \Gamma_0 \qquad (3)$$

$$\mathbf{u}=\{6U(H-y)y/H^2,\ 0\} \qquad \text{at } \Gamma_{in} \qquad (4)$$

$$\mu(\nabla\mathbf{u}+(\nabla\mathbf{u})^T)-\mathbf{I}p)=\mathbf{0} \text{ and } p=0 \qquad \text{at } \Gamma_{out} \qquad (5)$$

$$\mu(\nabla\mathbf{u}+(\nabla\mathbf{u})^T)-\mathbf{I}p)=\mathbf{0} \qquad \text{at } \Gamma_s \qquad (6)$$

In order to easily compare results the Reynolds number is introduced as $Re=\frac{\rho UH}{\mu}$, where U is the mean inlet flow speed and H is the height of the domain (here $H=1$). The secondary port is located in the bottom of a small appendix to the main flow domain. This ensures that the design domain is not directly influenced by the applied boundary condition.

The model is discretized using bilinear finite elements which do not fulfill the LBB-conditions. This is alleviated by the introduction of GLS stabilization on the weak form equations (Hauke and Hughes, 1994). The stabilization is

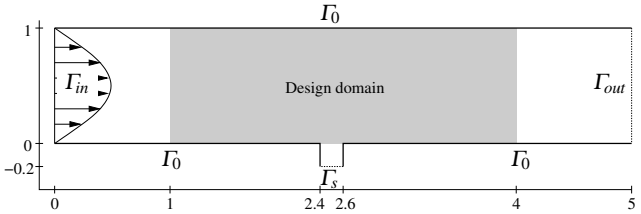

Fig. 2 Problem setting considered. The inflow (left, Γ_{in}) is a fully developed laminar profile with mean flow U and the outlet boundary (right, Γ_{out}) is modeled as stress free and $p = 0$, while the secondary flow port, Γ_s, is modeled with a stress free condition. The remaining thick solid line boundaries, Γ_0, have no-slip condition.

furthermore needed in order to resolve steep solution gradients avoiding the need for extremely fine meshes. The design results presented are based on a regular mapped mesh consisting of 50400 square elements with side length $h = 0.01$ i.e. 300×100 elements in the design domain.

2.1 Optimization

The flow component geometry which is subject to design optimization should be able to suck in fluid from the secondary flow port. This is possible if the inertia of the fluid flow is large enough to create a local low static pressure zone. Following Bernoulli's equation for inviscid flow theory such a scenario can be created if the fluid velocity is increased, leading to an increase in the dynamic pressure which results in a lower static pressure.

The objective of the optimization should be to maximize the amount of secondary fluid entering the flow component and leaving through the outlet. This can be formulated either as maximizing the flow through the secondary port Γ_s, maximizing the flow through the outlet port Γ_{out} or even by minimizing the pressure at the secondary port Γ_s, yielding the objective functions

$$\Phi_1 = -\int_{\Gamma_s} \mathbf{u}\cdot\mathbf{n}\,\mathrm{d}\Gamma \tag{7}$$

$$\Phi_2 = \int_{\Gamma_{out}} \mathbf{u}\cdot\mathbf{n}\,\mathrm{d}\Gamma \tag{8}$$

$$\Phi_3 = \int_{\Gamma_s} p\,\mathrm{d}\Gamma \tag{9}$$

where $\mathbf{n}$ is the outward pointing normal vector.

As the flow model is based on a known prescribed velocity profile and thus a known flow rate the resulting pressure drop across the component might be high for well performing dosing units. In order to investigate the trade-off between the cost (pressure drop) and the performance measured by the objective function, a pressure drop constraint is introduced and yields

$$g = \frac{\int_{\Gamma_{in}} p\mathrm{d}\Gamma}{\gamma\int_{\Gamma_{in}} p_{ref}\mathrm{d}\Gamma} - 1 \leq 0 \tag{10}$$

where p_{ref} references to the pressure in an empty pipe design and γ is the control parameter for the allowed pressure drop.

The optimization problem is formulated as a nested optimization problem yielding

$$\max_{\xi\in\mathbb{R}^N} \quad \Phi \tag{11}$$

$$s.t. \quad \text{Navier-Stokes equations (1), (2)} \tag{12}$$

$$g \leq 0 \tag{13}$$

$$0 \leq \xi \leq 1 \qquad \text{for } i = 1...N \tag{14}$$

where ξ is the design field which is a spatial field represented by one design variable for each finite element. The nested formulation is usually applied in topology optimization as it ensures that the physics in every design iteration is modeled correctly. Furthermore, it yields the possibility to abort the optimization procedure at any intermediate iteration and, assuming that the design is feasible, achieve an optimized design

The gradient information (sensitivities) that are needed to drive the optimization process is obtained using the adjoint method (Michaleris et al, 1994). It involves a single linear system solve for each functional i.e. objective or constraint function and is generally less computationally demanding than obtaining the non-linear flow problem solution.

The optimization problem is solved by applying the Method of Moving Asymptotes (MMA) by Svanberg (1987) and the optimization has been terminated using a design change criterion $\|\xi^{(k)} - \xi^{(k-1)}\|_\infty < 0.01$ that is a maximum 1% design change between two consecutive optimization iterations (k is the iteration counter) or in the case of design iterations exceeding 1000.

The FEM analysis is implemented using Comsol Multiphysics and interfaced from Matlab where Svanberg's implementation of MMA is used to drive the optimization process.

2.2 Design filter

When optimizing problems for low Reynolds number flows with a pressure drop constraint there is, contrary to problems in elasticity, not an inherent need for design regularization such as filtering. This is due to the nature of pressure losses which are minimized by minimizing the wetted perimeter i.e. multiple small channels are abandoned in favor for one large. When increasing the Reynolds number there is a tendency to obtain isolated *solid* elements within the design which yields poor physical modeling. A design filter is therefore applied to ensure an interrelation between adjacent design variables. The filter applied is a Helmholtz filter as introduced in Lazarov and Sigmund (2011) and it

provides a filtered design field $\widetilde{\xi}$ which is used for the interpolation of the inverse permeability i.e. $\alpha(\widetilde{\xi})$. The filter equation is

$$-r^2\nabla^2\widehat{\xi}+\widehat{\xi}=\xi \tag{15}$$

which is solved with homogeneous Neumann boundary conditions on all boundaries. The coefficient r defines the magnitude of diffusion and is related to the spatial filter radius (as used in e.g. the density filter (Bourdin, 2001; Bruns and Tortorelli, 2001)) by $R=r2\sqrt{3}$. The Helmholtz filter was applied as it is convenient to implement a PDE based filter in the framework of Comsol Multiphysics; however, traditional filters such as the density filter could also be applied. The ξ field constitutes the design variables bounded between zero and one as stated in (14) while $\widehat{\xi}$ is an intermediate field governed by the Helmholtz filter equation (15). A consequence is that the intermediate design field $\widehat{\xi}$ is now represented discretely in the nodes of the bi-linear elements leading to at least one *grey* element, but often several elements, in the transition from solid to fluid region. Therefore, in addition to the PDE-based filter, a thresholding is applied to ensure a relatively crisp boundary between the solid and fluid. Introducing a *tanh* based thresholding function (Wang et al, 2011) yields

$$\widetilde{\xi}_i=\frac{\tanh(\beta\eta)+\tanh(\beta(\widehat{\xi}_i-\eta)}{\tanh(\beta\eta)+\tanh(\beta(1-\eta))} \tag{16}$$

where the parameter η sets the thresholding value, here $\eta=0.5$, and β is the steepness of the thresholding function which for the limit $\beta\to\infty$ yields a sharp threshold. The material interpolation is getting increasingly nonlinear with increasing β; therefore, the value is increased gradually during the design process, where it initially is one and doubled every 40 iterations until it reaches a value of 64. See Wang et al (2011) or Guest et al (2011) for further discussion on the updating strategy of the steepness. For the presented results a filter with a radius $R=0.1$ is used. It should be noted that the filter does not introduce a length scale thus the relatively large filter radius still permits sharp corners and small details. If a length scale is needed the robust formulation (Wang et al, 2011) could be applied; however, this would restrict sharp corners at e.g. the nozzle throat.

2.3 Material interpolation

The design is enforced in the physical model by the introduction of an interpolation scheme similar to the one used by Borrvall and Petersson (2003) which yields

$$\alpha(\widetilde{\xi}_i)=\overline{\alpha}+(\underline{\alpha}-\overline{\alpha})\widetilde{\xi}_i\frac{1+q}{\widetilde{\xi}_i+q} \tag{17}$$

where the maximum and minimum inverse permeability is given by $\overline{\alpha}=10^6$ and $\underline{\alpha}=0$, respectively. The maximum value is chosen as a compromise between the ability to slow down the fluid and solver stability in terms of avoiding too large cancellation errors. The parameter q is a penalization parameter which influences the linearity of the interpolation and is in this work set to $q=0.01$. The interpolation shares characteristics with the RAMP scheme by Stolpe and Svanberg (2001) and the physical interpretation of the intermediate design values was investigated and compared with homogenization results in Andreasen and Sigmund (2013).

3 Results

Figure 3 shows the results of a minimization procedure using the objective Φ_3 (pressure in secondary inlet) for a design operating at $Re=20$ and allowing a pressure drop across the component of $\gamma=10$ times the empty pipe pressure drop. It is clearly seen that the design accelerates the fluid in the converging part of the nozzle until it reaches the throat. Hereafter the geometry diverges and the fluid slows down. From the streamline plot it is seen that fluid is definitely entering from the secondary port and leaving at the outlet. This can also be identified by inspecting the negative pressure (relative to outlet pressure) contour near the secondary port. The intensity of the two flows should not be compared based on the streamline distance as the number of streamlines for each port is fixed for visualization purposes.

It is apparent that there is a zone with recirculation just opposite the flow entering from the secondary port visualized by yellow streamlines. This is very natural as there is no possibility to drag in fluid from the top, hence some of the fluid along the upper boundary is dragged backwards by the low pressure to form the recirculation. A similar behavior is known from the often analyzed *backward facing step*.

The result shown was obtained using objective Φ_3 (pressure in secondary inlet), however similar design and performance have been obtained using Φ_1 (flow through secondary port) as the objective function. In order to study the usefulness of the three objective functions the design problem has been optimized for various Reynolds numbers and allowed pressure losses. All combinations using the parameter sets $Re=\{1,5,10,20,30\}$ and $\gamma=\{5,10,20,30\}$ have been optimized. The general tendency is that Φ_3 and Φ_1 performs almost equally well while there is difficulties in obtaining designs that makes fluid enter the secondary port when Φ_2 (outflow through outlet boundary) is used. The objective value history is shown in Fig. 4 where the sudden decreases in the objective function due to the continuation of the projection (β value) are clearly seen. For this case it is seen that already from iteration 300 the objective function value is close to the final value. The design does not

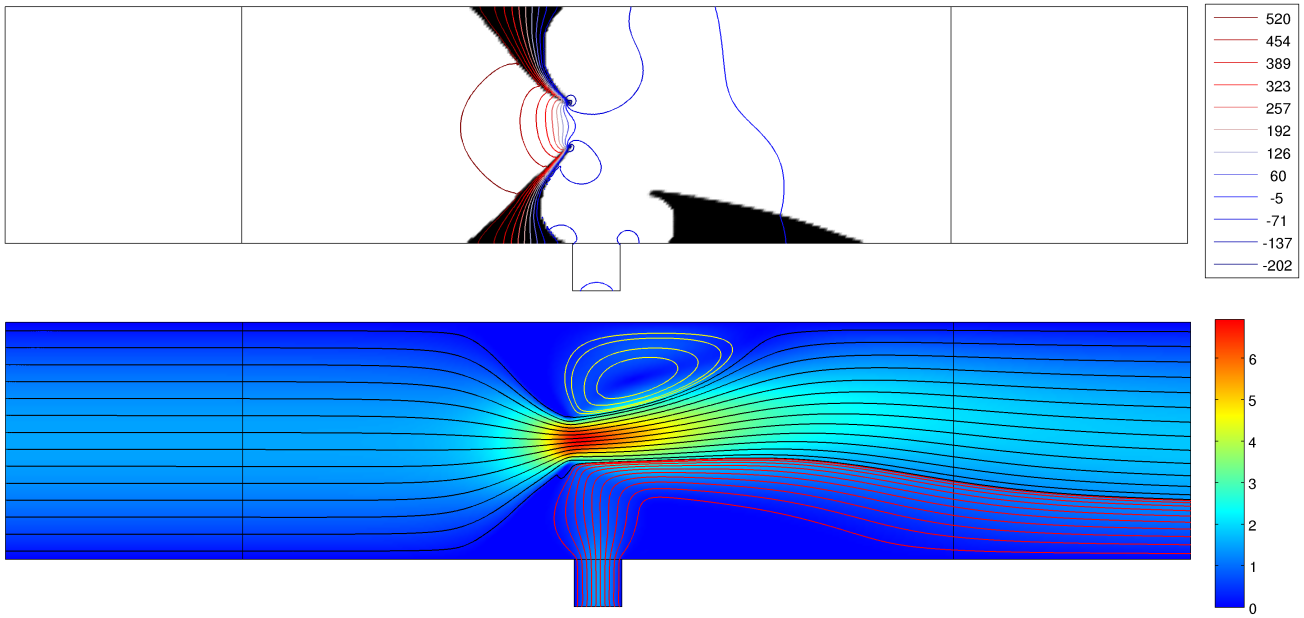

Fig. 3 Optimized flow geometry for $Re = 20$ and $\gamma = 10$. Upper: Component design with pressure contours (outlet is $p = 0$). Lower: Flow speed, inflow has mean speed 1, and streamlines seeded at the inlet port (black), secondary port (red) and the recirculation opposite the secondary port (yellow).

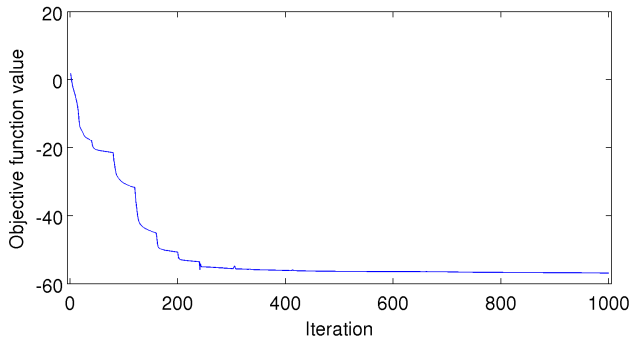

Fig. 4 Optimization history for the design in figure 3. The objective function Φ_3 is multiplied by 100 to ensure a proper magnitude of the objective for use with MMA. The β continuation for the projection is clearly seen by the sudden decreases in objective value.

change much during these last iterations where only small adjustments of the internal boundary occur.

3.1 Re and γ dependence on design

The range of parameters mentioned above yield 20 different design cases. In order to compare the performance of the obtained designs the *pumping coefficient* can be used. It measures the amount of fluid entering from the secondary port relative to the primary inflow

$$\varphi = \frac{Q_{out}}{Q_{in}^p} = \frac{\int_{\Gamma_{out}} \mathbf{u}\cdot\mathbf{n}\,\mathrm{d}\Gamma}{-\int_{\Gamma_{in}} \mathbf{u}\cdot\mathbf{n}\,\mathrm{d}\Gamma} \tag{18}$$

Since the inflow is fixed by definition for this problem, the measure is proportional to that of Φ_2. The objective function used for the study is Φ_3, minimization of pressure in the secondary port, which is also proportional to φ.

In figure 5 the pumping coefficient is plotted and determines the performance envelope for the individual aggregates operating at the point at which they have been optimized for. It can be seen that for increasing Re the performance is increased. There is more momentum in the incoming fluid that can be converted into a local low static pressure right after the nozzle. An increase in performance is also evident when allowing a larger pressure drop in the component; however, it is clearly seen that the performance is not increasing linearly with increased allowed pressure drop (γ) i.e. the efficiency of the optimized aggregates decline.

Figure 6 presents several of the optimized designs and it is indeed seen that the difference in topology is low while there is a much larger difference in the positioning of the features. All designs consist of a converging region and a diverging region. For the designs where the inflow Reynolds number is low the available momentum to create suction is also low and the designs seem to contain a small cavity in between the secondary port and the nozzle throat. For the $Re = 1$ designs, Fig. 6(a) and (b), this cavity gets larger (elongated) as the allowed pressure drop across the component is increased such that the throat is moved further downstream.

This tendency vanishes as the Reynolds number is increased and the throat is generally placed at the same horizontal position as where the secondary flow port begins.

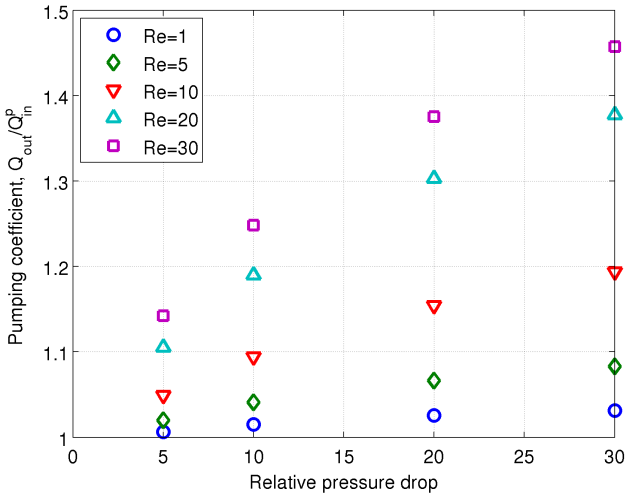

Fig. 5 Performance for the 20 design cases with varying Reynolds number, $Re = \{1,5,10,20,30\}$, and relative pressure drop, $\gamma = \{5,10,20,30\}$. The performance is the *pumping coefficient* measured as the rate of outflow, Q_{out} to primary inflow Q^p_{in}.

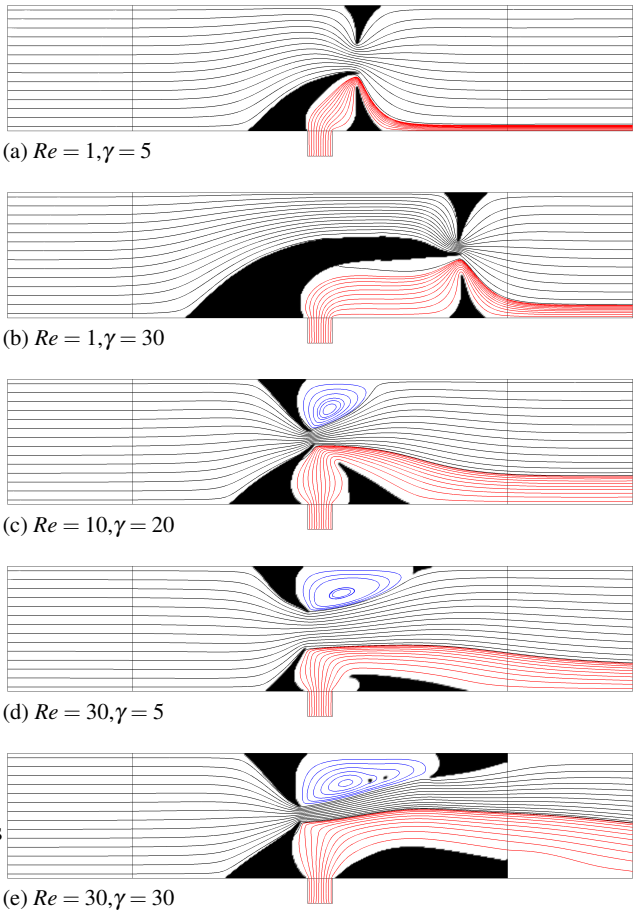

Fig. 6 Optimized designs for selected conditions. Black streamlines used for primary fluid (entering left) and red streamlines for the secondary fluid entering from below. Blue streamlines for recirculation zone opposite secondary port. The number of lines is selected for visualization.

Downstream of the throat, the low Reynolds number designs have a sudden expansion, while the *moderate* Reynolds number designs have what can be characterized as a diverging nozzle. It is in general asymmetric and for intermediate Reynolds numbers (Re=10) one-sided, see Fig. 6(c). The $Re = 30$ designs in Fig. 6(d) and (e) both have an unsymmetrical diverging nozzle and the latter even has two islands of solid material. These are placed in the low speed region of the fluid recirculation zone opposite the secondary port. The placement of two such islands of solid material might indicate that the optimization is not working well however, the design has been evaluated both with and without these islands and performed best with them. The performance decrease by removing them was 0.24% while the inlet pressure was decreased by 0.12% i.e. very minor changes. Inspecting the sensitivities of the objective function revealed that it would be favorable to introduce more solid material around the isles however, the sensitivities with respect to the pressure drop constraint had the opposite sign. This left the optimizer in a local minimum and finally terminated. Furthermore, the optimizer was restarted from the design where the islands had been removed to investigate if a better design could be obtained however, unsuccessfully. It is furthermore seen that the design is restricted spatially by the design domain boundary such that the diverging nozzle is truncated and two minor steps introduce a recirculation. For further designs in this limit a design domain redefinition may be considered.

In order to cross check the results of the optimization, all designs are reevaluated at all Reynolds numbers. The result of this study should work as a cross check to reveal if there are designs that perform better within a wide range of conditions. The resulting data is visualized in Fig. 7 where the designs that were optimized are identified with markers while all post evaluations of the designs are plotted as lines. From the figure it is seen that none of the optimized designs perform better at another set of conditions than the design optimized at these conditions. This is of course to be expected but not always the case, when optimizing general non-convex problems. The obtained designs may constitute either local minima or maybe not even stationary points as the optimizer could be unable to solve the problem until a KKT-point is reached.

Even though the designs are obtained for specific operation conditions they may be operated under slightly varying conditions. It is therefore interesting to investigate the performance for neighbouring operating points. From Fig. 7 is is also seen that the designs optimized for low Reynolds numbers also work reasonably for higher Reynolds numbers. The opposite is however, more problematic as the performance tends to drop quickly for the designs obtained at

larger Reynolds numbers when evaluated at lower values. It is furthermore interesting that when Re is increased the designs obtained for $Re = 20$ and $Re = 30$ the performance is first increasing and then decreasing while the tendency for the designs obtained for $Re = 5$ and $Re = 10$ seems to be a steady increase in performance with increasing Re.

It should be noted that due to the assumption of steady-state not all designs can be evaluated for the whole relative pressure drop range. Some designs are optimized for flow conditions which are on the limit of unstationary flow thus the solver is unable to converge to a steady-state solution.

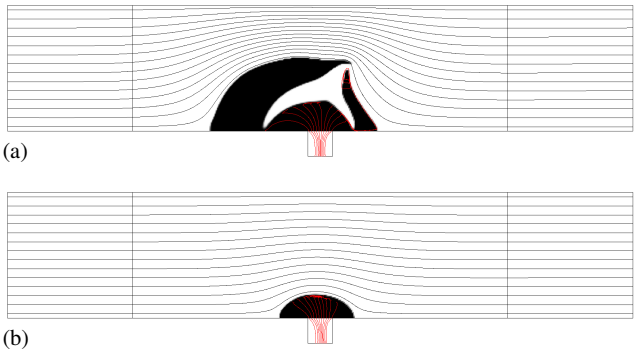

Fig. 8 Designs obtained for lower limit conditions $Re = 1$ $\gamma = 5$ using Φ_1 (a) and Φ_2 (b). The optimizer is unsuccessful in reopening the secondary port.

3.2 Observations during the optimization

The objective is to maximize the amount of secondary flow entering the component irrespectively which of the objective functions that is in use. The general tendency is that the optimizer at first tries to close the secondary flow port as it, for most conditions, works as a sink rather than a source. This initiates a buildup of solid material that closes the port and improves the objective. However, in order to improve the objective further, the port needs to be reopened such that secondary fluid can enter the component. The occasional inability to succeed in this is illustrated in Fig. 8 where Φ_1 and Φ_2, respectively, were used for optimization.

In this respect, the optimization problem shows similarities with that of topology optimization of compliant mechanism problems e.g. the force inverter Sigmund (1997) that initially tries to isolate input and output but thereafter need to connect the two to obtain the necessary flexibility to actuate. The procedure of *switching sign* of the objective has previously been reported as troublesome which is to some extend also the case for the present design optimization problem.

The problem is most pronounced for the lowest Reynolds numbers as it is indeed difficult to reach a design that initiates suction from the secondary port. This is exactly where the difference in choice of objective function shows up. Ideally all three objective functions should lead to the same design as the fluid is considered incompressible. There are, however, clear differences in how the optimization proceeds. While using the objective function, Φ_2, where the total outflow of the component is optimized, the optimizer has severe problems in initiating an entering flow at the secondary port. When the secondary port is first closed to avoid fluid exiting early in the design process it is not prone to be reopened again. This problem is also present for the $Re = 1, \gamma = 5$ case in combination with Φ_1. Constructing the initial design such that it already has fluid entering from the secondary port is of course one workaround; however, not very general.

For all objective functions various alternative initial designs have been applied to investigate how to trigger the functionality of making fluid enter from the secondary port. For objective functions Φ_1 and Φ_3 an initial all fluid design is generally working fine. Another important aspect is the scaling of the objective function. For objective values around 0, the sensitivities of the potential design changes may also be very small and potentially influence the optimization algorithm behavior.

3.3 Problems of limited mixing - perspectives of 3D optimization

Apart from the ability to dispense the secondary fluid, a further quality of the component would be its ability to ensure a proper mixing of the two fluids. Inspecting the streamlines in Fig. 6 it is obvious that convective mixing is not pronounced for these designs. The mixing is present at the interface between the primary and secondary fluid and dominated by diffusion. This is a limitation of a 2D flow model since no streamlines can cross or entangle into and out of the plane. However, even for 3D problems a proper mixing would have a cost in terms of increased internal friction due to the needed secondary motion. The problem of optimizing the mixing was studied in Andreasen et al (2009). It is therefore not expected that the presented formulation would ensure proper mixing in a 3D context either. The allowed pressure drop over the component i.e. the supplied power would need to split into the two sub processes of secondary fluid suction and mixing, thus ensuring proper mixing would decrease the dispensing ability.

4 Conclusion

A methodology for optimizing dosing components in laminar flows of low to moderate Reynolds numbers using topology optimization has been developed and demonstrated. The resulting designs rely on the principles also known from

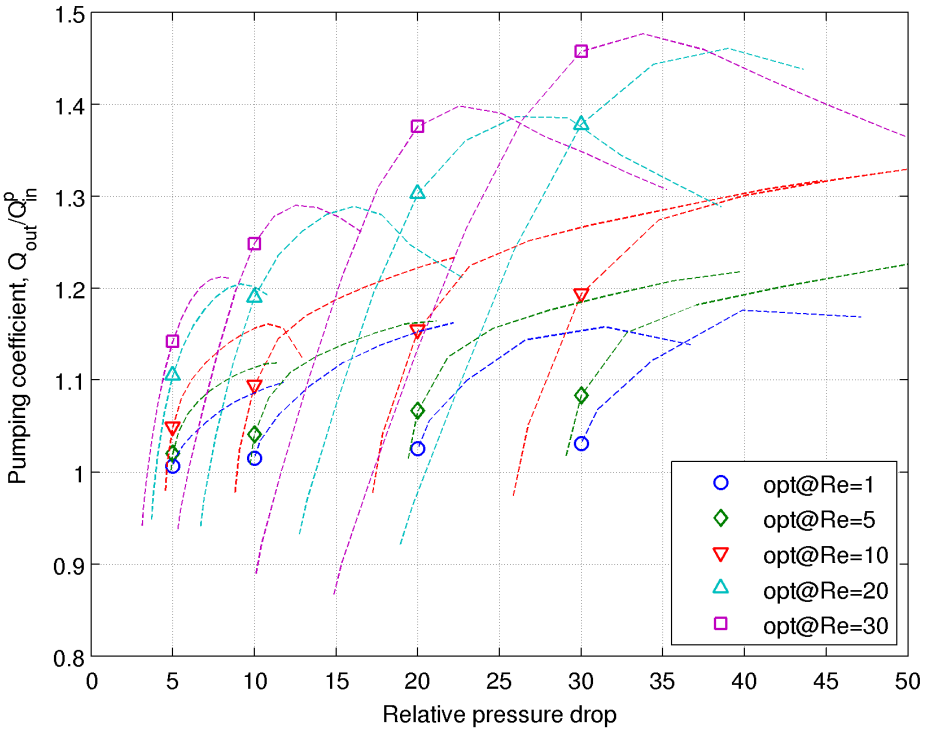

Fig. 7 Performance cross check with other optimized designs all obtained using objective Φ_3. Each design, obtained at the point identified by the marker, is reevaluated at a range of Reynolds numbers $\{1, 5, 10, 15, 20, , ... ,60\}$ and results are plotted as lines.

venturi nozzles where the dynamic pressure is increased and the static pressure decreased in the throat. This low static pressure allows the secondary flow to enter the flow component and thus be a part of the fluid leaving it further downstream. The ability to mix the primary and secondary phase is limited due to the nature of plane flows.

The paper furthermore discusses the difficulty of designing dosing components operating at low Reynolds numbers as the inertia in these cases is very low and the choice of objective function seems to be important for the successful application of the procedure.

Acknowledgements The author would like to thank Professor K. Svanberg, KTH, Sweden for use of his MMA implementation and the TopOpt group for fruitful discussions on the topic.

References

Alexandersen J, Aage N, Andreasen CS, Sigmund O (2014) Topology optimisation for natural convection problems. International Journal for Numerical Methods in Fluids 76(10):699–721, DOI 10.1002/fld.3954

Alexandersen J, Sigmund O, Aage N (2016) Large scale three-dimensional topology optimisation of heat sinks cooled by natural convection. UNDER REVIEW Preprint available on arXiv:1508.04596

Andreasen CS, Sigmund O (2013) Topology optimization of fluid-structure-interaction problems in poroelasticity. Computer Methods in Applied Mechanics and Engineering 258(0):55 – 62, DOI 10.1016/j.cma.2013.02.007

Andreasen CS, Gersborg AR, Sigmund O (2009) Topology optimization of microfluidic mixers. International Journal For Numerical Methods In Fluids 61(5):498–513, DOI 10.1002/fld.1964

Andreasen CS, Aage N, Madsen TBS (2014) Topology optimization of flow machinery. In: Karlaftis MG, Lagaros ND, Papadrakakis M (eds) Proceedings of 1st International Conference on Engineering and Applied Sciences Optimization, National Technical University of Athens, p 1964

Bendsøe M, Sigmund O (2003) Topology Optimization - Theory, Methods and Applications, 2nd edn. Springer Verlag

Bendsøe MP, Kikuchi N (1988) Generating optimal topologies in structural design using a homogenization method. Computer Methods in Applied Mechanics and Engineering 71(2):197–224, DOI 10.1016/0045-7825(88)90086-2

Borrvall T, Petersson J (2003) Topology optimization of fluids in Stokes flow. International Journal for Numerical Methods in Fluids 41(1):77–107, DOI 10.1002/fld.426

Bourdin B (2001) Filters in topology optimization. International Journal for Numerical Methods in Engineering 50:2143–2158

Brinkman HC (1947) A calculation of the viscous force exerted by a flowing fluid on a dense swarm of particles. Applied Scientific Research Section A-mechanics Heat Chemical Engineering Mathematical Methods 1(1):27–34, DOI 10.1007/BF02120313

Bruns T, Tortorelli D (2001) Topology optimization of nonlinear elastic structures and compliant mechanisms. Computer Methods in Applied Mechanics and Engineering 190:3443–3459

Deng Y, Liu Z, Zhang P, Liu Y, Wu Y (2011) Topology optimization of unsteady incompressible Navier–Stokes flows. Journal of Computational Physics 230(17):6688–6708, DOI 10.1016/j.jcp.2011.05.004

Dvorák V (2006) Shape optimization of axisymmetric ejector. In: ECCOMAS CFD 2006: Proceedings of the European Conference on Computational Fluid Dynamics, Egmond aan Zee, The Netherlands, September 5-8, 2006, Delft University of Technology; European Community on Computational Methods in Applied Sciences (ECCOMAS)

Evgrafov A, Pingen G, Maute K (2008) Topology optimization of fluid domains: kinetic theory approach. ZAMM - Journal of Applied Mathematics and Mechanics / Zeitschrift für Angewandte Mathematik und Mechanik 88(2):129–141, DOI 10.1002/zamm.200700122

Fan J, Eves J, Thompson H, Toropov V, Kapur N, Copley D, Mincher A (2011) Computational fluid dynamic analysis and design optimization of jet pumps. Computers & Fluids 46(1):212 – 217, DOI 10.1016/j.compfluid.2010.10.024, 10th {ICFD} Conference Series on Numerical Methods for Fluid Dynamics (ICFD 2010)

Gersborg-Hansen A, Sigmund O, Haber R (2005) Topology optimization of channel flow problems. Structural and Multidisciplinary Optimization 30(3):181–192, DOI 10.1007/s00158-004-0508-7

Guest J, Asadpoure A, Ha SH (2011) Eliminating beta-continuation from heaviside projection and density filter algorithms. Structural and Multidisciplinary Optimization 44(4):443–453, DOI 10.1007/s00158-011-0676-1

Hauke G, Hughes T (1994) A unified approach to compressible and incompressible flows. Computer Methods in Applied Mechanics and Engineering 113(3-4):389–395, DOI 10.1016/0045-7825(94)90055-8

Hu H, Kobayashi T, Saga T, Taniguchi N, Liu H, Wu S (1999) Research on the rectangular lobed exhaust ejector/mixer systems. Transactions-Japan society for aeronautical and space sciences 41:187–194

Kreissl S, Maute K (2012) Levelset based fluid topology optimization using the extended finite element method. Structural and Multidisciplinary Optimization 46(3):311–326, DOI 10.1007/s00158-012-0782-8

Kreissl S, Pingen G, Evgrafov A, Maute K (2010) Topology optimization of flexible micro-fluidic devices. Structural and Multidisciplinary Optimization 42:495–516, DOI 10.1007/s00158-010-0526-6

Kreissl S, Pingen G, Maute K (2011) Topology optimization for unsteady flow. International Journal for Numerical Methods in Engineering 87(13):1229–1253, DOI 10.1002/nme.3151

Lazarov BS, Sigmund O (2011) Filters in topology optimization based on {H}elmholtz-type differential equations. International Journal for Numerical Methods in Engineering 86(6):765–781, DOI 10.1002/nme.3072

Marck G, Nemer M, Harion JL (2013) Topology optimization of heat and mass transfer problems: Laminar flow. Numerical Heat Transfer, Part B: Fundamentals 63(6):508–539, DOI 10.1080/10407790.2013.772001

Michaleris P, Tortorelli DA, Vidal CA (1994) Tangent operators and design sensitivity formulations for transient non-linear coupled problems with applications to elastoplasticity. Int J Numer Meth Engng 37(14):2471–2499, DOI 10.1002/nme.1620371408

Nørgaard S, Sigmund O, Lazarov B (2016) Topology optimization of unsteady flow problems using the lattice boltzmann method. Journal of Computational Physics 307:291–307, DOI 10.1016/j.jcp.2015.12.023

Okkels F, Bruus H (2007) Scaling behavior of optimally structured catalytic microfluidic reactors. Physical Review E 75(1):016,301, DOI 10.1103/PhysRevE.75.016301

Othmer C (2008) A continuous adjoint formulation for the computation of topological and surface sensitivities of ducted flows. International Journal for Numerical Methods in Fluids 58(8):861–877, DOI 10.1002/fld.1770

Pingen G, Evgrafov A, Maute K (2007) Topology optimization of flow domains using the lattice Boltzmann method. Structural and Multidisciplinary Optimization 34(6):507–524, DOI 10.1007/s00158-007-0105-7

Pironneau O (1973) On optimum profiles in stokes flow. Journal of Fluid Mechanics 59:117–128, DOI 10.1017/S002211207300145X

Romero J, Silva E (2014) A topology optimization approach applied to laminar flow machine rotor design. Computer Methods in Applied Mechanics and Engineering 279(0):268 – 300, DOI 10.1016/j.cma.2014.06.029

Sigmund O (1997) On the Design of Compliant Mechanisms Using Topology Optimization. Mechanics of Structures and Machines 25(4):493–524, DOI 10.1080/08905459708945415

Stolpe M, Svanberg K (2001) An alternative interpolation scheme for minimum compliance topology optimization. Structural and Multidisciplinary Optimization 22(2):116–

124, DOI 10.1007/s001580100129

Svanberg K (1987) The method of moving asymptotes - a new method for structural optimization. International Journal for Numerical Methods in Engineering 24(2):359–373, DOI 10.1002/nme.1620240207

Wang F, Lazarov B, Sigmund O (2011) On projection methods, convergence and robust formulations in topology optimization. Structural and Multidisciplinary Optimization 43(6):767–784, DOI 10.1007/s00158-010-0602-y

Yoon GH (2010a) Topological design of heat dissipating structure with forced convective heat transfer. Journal of Mechanical Science and Technology 24(6):1225–1233, DOI 10.1007/s12206-010-0328-1

Yoon GH (2010b) Topology optimization for stationary fluid-structure interaction problems using a new monolithic formulation. International Journal for Numerical Methods in Engineering 82(5):591–616, DOI 10.1002/nme.2777